ACS OMEGA

http://pubs.acs.org/journal/acsodf

Article

Cytotoxic, Antidiabetic, and Antioxidant Study of Biogenically Improvised *Elsholtzia blanda* and Chitosan-Assisted Zinc Oxide Nanoparticles

Athisa Roselyn Maheo, Scholastica Mary Vithiya B, Augustine Arul Prasad T,* V. L. Mangesh, Tamizhdurai Perumal,* Wahidah H. Al-Qahtani, and Mani Govindasamy*

Cite This: *ACS Omega* 2023, 8, 10954−10967

Read Online

ACCESS | Metrics & More | Article Recommendations

ABSTRACT: In the present study, we have improvised a biogenic method to fabricate zinc oxide nanoparticles (ZnO NPs) using chitosan and an aqueous extract of the leaves of *Elsholtzia blanda*. Characterization of the fabricated products was carried out with the help of ultraviolet−visible, Fourier transform infrared, X-ray diffraction, field emission scanning electron microscopy, high-resolution transmission electron microscopy, selected area electron diffraction, and energy-dispersive X-ray analyses. The size of the improvised ZnO NP measured between 20 and 70 nm and had a spherical and hexagonal shape. The ZnO NPs proved to be highly effective in the antidiabetic test as the sample showed the highest percentage of enzyme inhibition at 74% ± 3.7, while in the antioxidant test, 78% was the maximum percentage of 2,2-diphenyl-1-picrylhydrazyl hydrate scavenging activity. The cytotoxic effect was investigated against the human osteosarcoma (MG-63) cell line, and the IC_{50} value was 62.61 μg/mL. Photocatalytic efficiency was studied by the degradation of Congo red where 91% of dye degradation was observed. From the various analyses, it can be concluded that the as-synthesized NPs may be suitable for various biomedical applications as well as for environmental remediation.

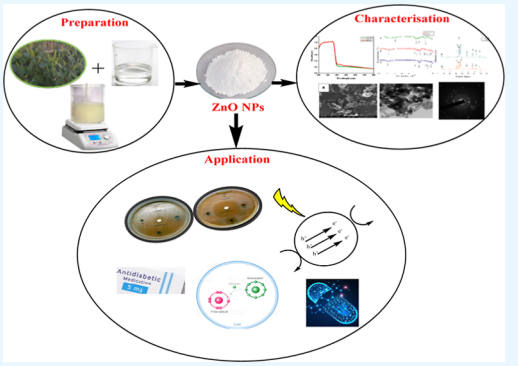

1. INTRODUCTION

Fabrication of low-cost, simple, and nonhazardous nanoparticles (NPs) is gaining huge momentum with an ever-new product on the rise. Their small size and large surface area are their greatest advantages. Advancement in nanotechnology is indispensably associated with modernization and advancement in all spheres of human existence. The impact of nanotechnology includes in science, drugs, healthcare, machinery, space programs, information technology, electronics, optics, catalysis, environmental remediation, agricultural practices, and so forth. Hollow C@SnS_2/SnS nanocomposites used as electrocatalyst,[1] ZnS−Ag_2S NPs used for photothermal detection of a transcription factor,[2] fluorescent ZnO−Au nanocomposite as a probe to elucidate DNA interaction,[3] and hybrid Ag−Fe_3O_4 obtained with the aid of *Rubia tinctorum* as a reductant and a stabilizing agent[4] are some examples on the importance of nanotechnology.

Previously, many NPs with excellent biological as well as chemical applications have been synthesized via chemical/physical methods. This, however, has the disadvantage of using hazardous substances. The green method of synthesizing NPs is gaining ground in recent years. An alternative to the conventional method of NP synthesis is the cleaner and greener method involving bacteria, algae, yeast, actinomycetes, or plant parts as this entails no perilous or hazardous substances.[5] Size-dependent antibacterial activity of ZnO NPs that were synthesized using the leaf extract of *Dysphania ambrosioides* was observed.[6] A comparative study was made between green-synthesized and chemically synthesized copper oxide NPs by Sabeena et al.[7] Many metallic and metal oxide NPs such as palladium NPs,[8,9] silver NPs,[10] copper oxide NPs,[11,12] and bimetallic copper−silver NPs[13] are synthesized using different plant parts which have very useful biological and chemical applications. An added advantage to the use of plant parts is that the phytochemicals from plants enhance the properties of the NPs. The biomolecules that are found in plant parts serve as excellent reducing, stabilizing, and capping agents in the green manufacturing of NPs. They are directly responsible for reducing the metal precursors to their nanosize. Akhavan et al. used ginseng, a herbal medicine, as a green reductant to obtain reduced graphene sheets.[14] The leaf extract of *Eucalyptus*

Received: November 24, 2022
Accepted: February 6, 2023
Published: March 15, 2023

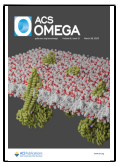

globulus was used as a stabilizer to synthesize copper oxide NPs.[15] The zinc oxide NPs, synthesized by the mediation of the leaf extract of *Anoectochilus elatus,* possessed strong antimicrobial, anti-inflammatory, and antioxidant properties.[16] Faisal et al. synthesized zinc oxide NPs using the aqueous fruit extract of *Myristica fragrans* which had good antibacterial, antidiabetic, antioxidant, antiparasitic, and larvicidal properties.[17]

Engineered metal oxide NPs such as copper oxides,[18] manganese oxides,[19] titanium oxides,[20] aluminium oxides,[21] iron oxides,[22] cerium oxides,[23] and silver oxides[24] are among the most common NPs having unique properties and applicability in diverse fields. Behaving as a good n-type semiconductor, ZnO NPs are gaining significant interest among researchers. This is attributed to their unique properties and applicability in varied fields due to their nontoxic nature, low cost, high catalytic activity, biocompatibility,[25] and so forth. Another important characteristic nature of ZnO is its UV filtering capacity which is why it is widely used in cosmetic products. Besides, ZnO also plays a significant role in many medicinal uses such as wound-healing, anticancer, antimicrobial, anti-inflammatory, and drug delivery.[26] Recent work showed the synthesis of *Rosmarinus officinalis*-mediated Ca−ZnO-based nanoghosts which had significant biological applications.[27] Rajabi et al. synthesized ZnO NPs using the aqueous extract of *Suaeda aegyptiaca* which exhibited good antimicrobial, antifungal, and antioxidant properties.[28] The adsorbance of carcinogenic bisphenol-A from the water bodies by chitosan/gelatin loaded with ZnO NPs/*Chlorella vulgaris* is a good example of environmental remediation by NPs.[29]

Elsholtzia blanda, commonly known as the pleasant Himalayan mint, is an aromatic herb with plentiful volatile oils as its main constituent. Traditionally, fresh leaves are eaten to lower blood pressure and in treating dysentery, stomach pain, and other gastrointestinal disorders. They are also found to possess antibacterial, antioxidant, cardioprotective, and reno-protective effects.[30] Besides their medicinal uses, the plant is also used as a vegetable and spice. Flavonoids, particularly luteolin, are found to be the major constituents of the Elsholtzia family.[31] Phenylpropanoids, terpenoids, and cyanogenic glycosides are other biomolecules found in the plant.[32]

Chitosan is obtained by deacetylation of chitin, which in turn is obtained from the exoskeleton of crustaceans. The hydroxyl amino groups in chitosan are mainly responsible for their various properties, such as reducing activity, which leads to the formation of NPs or their ability to bond with other metal or metal oxides. As a result, its physicochemical and biological qualities are improved.[33,34] As a coordinating agent, chitosan also helps in the nucleation and growth of the NPs.[35] Being biodegradable and void of toxicity, it is widely used in tissue engineering and as antibacterial agents. The primary $-NH_2$ group found in chitosan plays a pivotal role in many of its activities.

Previous works in the literature suggest that plant components can be used to synthesize ZnO NPs, some of which are *Eriobotrya japonica*,[36] *Asparagus racemosus*,[37] *Cayratia pedata*,[38] *Cassia auriculata*,[39] *Averrhoa carambola*,[40] *Parthenium hysterophorus*,[41] *Albizia lebbeck*,[42] *Mentha pulegium*,[43] *Carissa edulis*,[44] and *Aloe socotrina*.[45] Chitosan and plant extract-mediated metal oxide NPs in the literature include MgO,[46] TiO_2,[47] CuO,[48] and ZnO.[49]

The present work gives an insight into the investigative study of the antioxidant, antidiabetic, cytotoxic, and photocatalytic efficiencies of ZnO NPs synthesized through the mediation of the leaf extract of *E. blanda* and chitosan. Very few works are reported in the literature on the dual use of leaf extract and chitosan to synthesize NPs. The novelty of our work lies in the method which followed a purely green scheme involving no hazardous substances and which was time- and cost-effective.

2. EXPERIMENTAL SECTION

2.1. Chemicals. Zinc nitrate hexahydrate $[Zn(NO_3)_2 \cdot 6H_2O]$ was purchased from Sisco Research Laboratories Pvt. Ltd. Maharashtra, India, chitosan was purchased from Sisco Research Laboratories Pvt. Ltd., and sodium hydroxide (NaOH) and acetic acid (CH_3COOH) were obtained from Spectrum Reagents and Chemicals Pvt. Ltd. Edayar, Cochin. They were of analytical grade and did not require any additional purification.

2.2. Leaf Collection and Extract Preparation. Fresh leaves of *E. blanda* were gathered from Punanamei village, Manipur, India in September. They were properly cleansed in flowing tap water to remove any harmful or undesired substances before being dried in the shade at room temperature. The leaves were taxonomically authenticated at the Department of Botany, D.G.Vaishnav College Chennai, Tamil Nadu, India.

5 g of the leaves that were shade-dried were placed in a 200 mL beaker which had 100 mL of double-distilled water and heated for 30 min at 85 °C. After cooling the mixture, Whatman filter paper no. 1 was used to filter it, and the filtrate was employed as the plant extract for the biosynthesis of the required NPs.

2.3. Biosynthesis of ZnO NPs. 20 mL of the leaf extract and 60 mL of 0.05 M zinc nitrate solution were mixed and stirred at 70 °C for 30 min using a magnetic stirrer before adding 2.0 M NaOH dropwise till pH ∼ 9 was attained. 20 mL of chitosan solution obtained by dissolving 1 g of chitosan in 100 mL of 1% acetic acid was further added to the mixture, and stirring was continued for another 3 h at 80 °C. Color change was noticed from being colorless to brownish before it finally became yellowish-white jelly. This method helped in obtaining *E. blanda* and chitosan-assisted ZnO NPs (ZPCB). *E. blanda*-assisted ZnO NPs (ZPB) were also prepared similarly without adding chitosan to the mixture. The formed NPs were washed thoroughly with double-distilled water, filtered, and dried in an oven for 4 h at 200 °C. A schematic illustration of the procedure and mechanism involved is shown in Figure 2.

2.4. Characterization. The various characterization techniques employed to characterize the biosynthesized NPs were UV−vis spectroscopy, Fourier transform infrared (FTIR) spectroscopy, X-ray diffraction (XRD), scanning electron microscopy (SEM), energy dispersive X-ray analysis (EDAX), transmission electron microscopy (TEM), and selected area electron diffraction (SAED).

2.4.1. UV−Vis Spectroscopy. A noticeable change was noted in the solution's color as it became yellowish-white, indicating the formation of NPs. UV−visible spectra using a wavelength spanning from 200 to 800 nm with a 1 nm data interval were used to analyze the optical property and confirm the formation of ZnO NPs. It was measured employing a UV spectrophotometer (Jasco V-670 Serial no. B072061154).

2.4.2. FTIR Spectra. The FTIR spectra were recorded using a Nicolet iS50 (Thermo Scientific, USA) spectrometer. In this, KBr pellets were used and the measurement was taken in the range of 4000−400 cm^{-1} with a resolution of 4 cm^{-1}. This helped in establishing the identity of the phytochemicals that

https://doi.org/10.1021/acsomega.2c07530
ACS Omega 2023, 8, 10954−10967

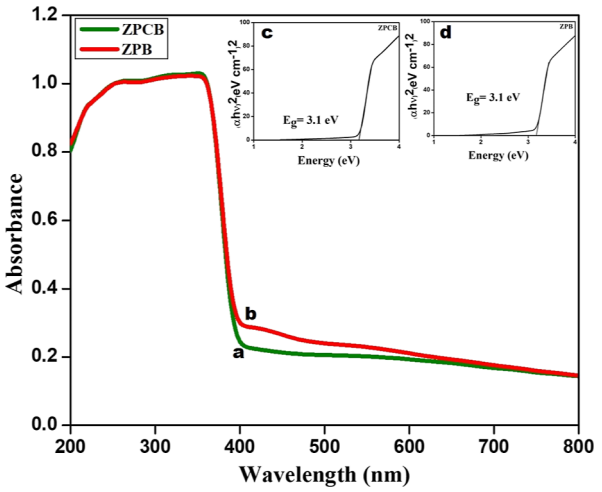

Figure 1. UV−vis absorption spectra of (a) ZPCB and (b) ZPB. Tauc's plot (inset) of (c) ZPCB and (d) ZPB.

helped in reducing, capping, and stabilizing the NPs as well as the Zn−O bonds.

2.4.3. XRD. The crystal phase, purity, and average crystal size were estimated with the help of XRD crystallography using a D8 ADVANCE (Bruker, Germany) diffractometer fitted with a 2.2 kW Cu-anode ceramic tube as the radiation source. The measurement was taken over the range of $2\theta = 10-90°$.

2.4.4. Field Emission SEM with EDAX. Surface morphology and particle size analyses were performed by SEM which was equipped with EDAX to analyze the elemental composition.

2.4.5. High-Resolution TEM with SAED. The structural morphology, shape, and size of the NPs were determined with the help of high-resolution transmission electron microscopy (HRTEM) combined with SAED for phase identification. The particles were scanned at an accelerating voltage of 200 kV.

2.5. Biological Activities. *2.5.1. Antidiabetic Potential (α-Amylase Assay).* Taking acarbose as the standard, the in vitro antidiabetic activity of ZnO NPs was investigated employing the inhibitory effect of α-amylase. Constraining the activity of α-amylase helps to reduce the glucose absorption rate as the enzyme plays a vital role in hydrolyzing the carbohydrates. The potential of ZnO NPs as an antidiabetic was analyzed through the alpha amylase assay using the approach described by Prasad et al. with few changes.[50] To 390 mL of phosphate buffer containing varied concentrations, that is, 5, 10, 15, 20, and 25 μg/mL of the sample solution, 10 μL of α-amylase solution (0.025 mg/mL) was added. The mixture was incubated for 10 min at 37 °C, and 100 μL of the starch solution was added as a substrate. Incubation was carried out for another hour before adding 0.1 mL of 1% iodine solution and 5 mL of double-distilled water. Taking acarbose as the control, the absorbance was studied at 565 nm. The percentage of enzyme inhibition was obtained using the formula

$$\% \text{ of inhibition} = \frac{A_c - A_s}{A_c} \times 100 \quad (1)$$

Here, A_c refers to the absorbance of the control and A_s to the absorbance of the sample.

2.5.2. Antioxidant Potential (DPPH Assay). The 2,2-diphenyl-1-picrylhydrazyl hydrate (DPPH) radical scavenging efficiency of the prepared NPs was compared with that of the standard ascorbic acid. 3 mL of methanolic 0.004% DPPH solution was mixed with different concentrations (5, 10, 15, 20, and 25 μg/mL) of the synthesized ZnO NPs. The mixture was shaken vigorously to attain homogeneity and was kept in the dark for half an hour at room temperature. The absorbance of the mixture was then measured at 517 nm with the help of a UV−Vis spectrophotometer (LMSP-UV1000B). The antioxidant activity (D) was further calculated using the equation

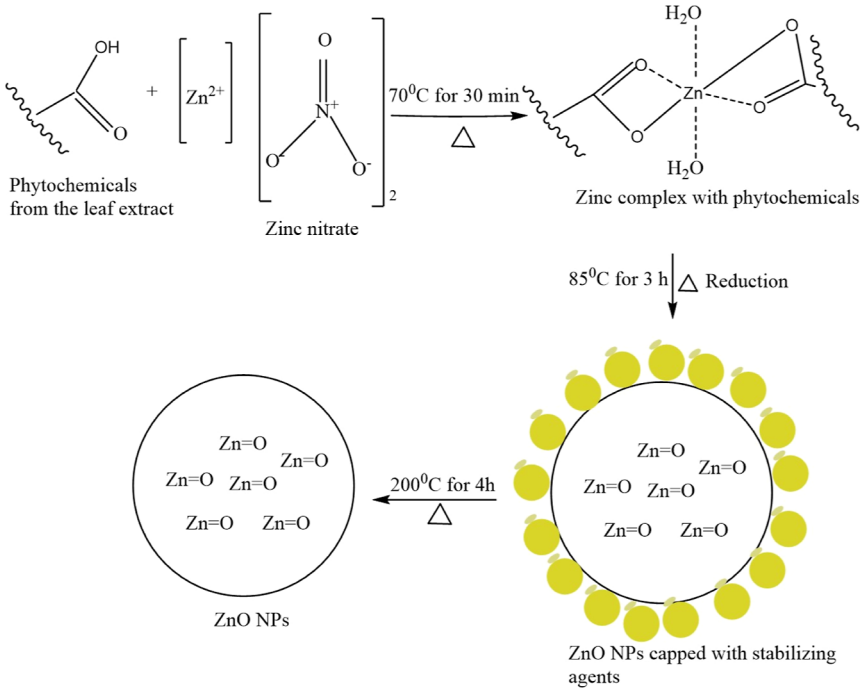

Figure 2. Hypothesized mechanism involved in the formation of ZnO NPs.

https://doi.org/10.1021/acsomega.2c07530
ACS Omega 2023, 8, 10954−10967

$$D\ (\%) = \frac{A_c - A_c}{A_c} \times 100 \quad (2)$$

where A_c and A_s are the absorbances of the control and sample, respectively.

2.5.3. Cytotoxicity Potential (MTT Assay). MG-63 cell line (human osteosarcomas cell) was utilized to investigate the cytotoxic potential of the biosynthesized ZnO NPs. MG-63 cell line was purchased from NCCS, Pune. DMEM medium which was supplemented with FBS (10%), penicillin (100 μg/mL), and streptomycin (100 μg/mL) was used to culture the cell lines and was incubated at 37 °C in an atmosphere of 5% carbon dioxide. The cells were then seeded in a 96-well tissue culture plate at a density of 1×10^5 cells/mL and left to stand for 24 h at 37 °C. The original medium was discarded, and ZPCB samples at varying concentrations were added to the well and placed in an incubator for a day. When the incubation was completed for 24 h, 20 μL of MTT (5 mg/mL) was further added to the wells and reincubated for another 4 h. At the end of 4 h of incubation, the medium was carefully removed and washed with 200 μL of phosphate-buffered saline before adding 100 μL of dimethyl sulfoxide to dissolve the formazan crystals. The plate was then shaken for 5 min for efficient mixing. The absorbance was finally recorded at 570 nm using a microplate reader, and the percentage of cell viability and IC_{50} value were calculated. The percentage of cell viability was calculated using the formula

$$\text{cell viability } \% = \text{test OD/control OD} \times 100 \quad (3)$$

2.6. Photocatalytic Potential. The photocatalytic potential of the biosynthesized ZnO NPs was evaluated by the decomposition of Congo red under light irradiation. The experiment was carried out using a double-beam UV−vis spectrophotometer (ELICO-SL218). For this purpose, a working solution of 100 μg/mL of the dye was prepared. Varying concentrations (10, 20, 30 40, and 50 μg) of ZnO NPs were then added to the working solution which had equal volumes and allowed to stand for 10 h. In another condition, keeping the concentration of the NPs constant, that is, 50 μg/mL, the working solution was exposed to light for varying lengths of time (0, 2, 4, 6, 8, and 10 h). The photocatalytic potential of the NPs was thus estimated centered on two factors, concentration and duration of time exposed to light. The absorbance was taken at Congo red absorption value which is 497 nm. The reactions were carried out in triplicate to get a concordant reading.

3. RESULTS AND DISCUSSION

3.1. UV−Vis. The UV−vis spectra of ZPCB and ZPB are shown in Figure 1. A strong absorption peak was observed at 356 nm in the spectra which is characteristic of ZnO NPs. The purity of the sample is confirmed by the occurrence of a single peak each for the two NPs without any additional peaks. The position of the absorption peak depends largely on the particle size, shape, and concentration. Similar results with absorption peaks ranging from 350 to 380 nm for ZnO NPs were reported in the literature.[51−53]

The optical band gap determined by using Tauc's plot [Figure 1 (inset)] showed a band gap of 3.1 eV for both the green-synthesized NPs. Previously reported band gap values ranged from 3.1 to 3.4 eV.[54−57]

3.2. Plausible Mechanism of Biosynthesis of ZnO NPs. Varied biomolecules found in the leaf extracts possess strong reducing, capping, and stabilizing properties. These are essential for the synthesis of NPs. The main phytochemicals found in the leaf extract of *E. blanda* are flavonoids, terpenoids, polyphenols, tannin, luteolin, and phenylpropanoids. The hydroxyl group found in these biomolecules forms a metal complex with the dispensed Zn^{2+} which on reduction and stabilization yields the desired product.[58] The hypothesized reaction that takes place in the process is shown in Figure 2.

3.3. FTIR. FTIR (Figure 3) shows evidence of functional groups found in biomolecules that were responsible for reducing

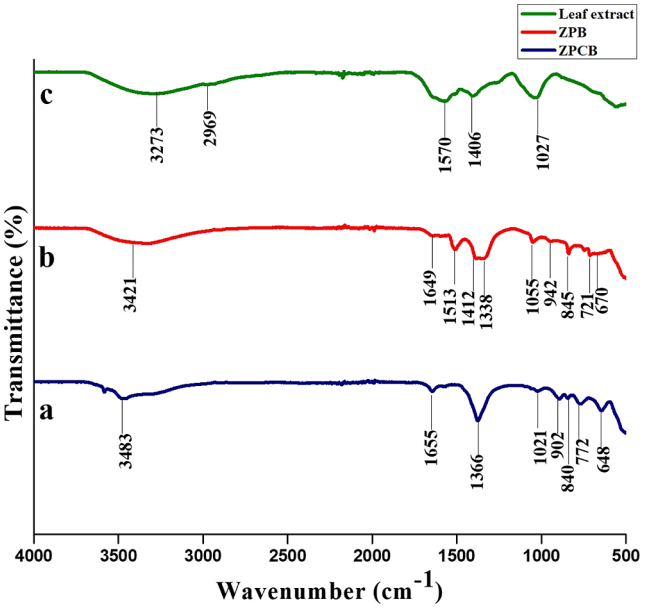

Figure 3. FTIR spectra of (a) ZPCB, (b) ZPB, and (c) plant extract.

the metal precursor to the desired product. Besides, the formation of the Zn−O bond too is confirmed by their characteristic absorption peak. In Figure 3a,b, the bands at 3421 and 3483 cm^{-1} corresponded to the stretching and bending vibrations of the OH group. The peaks at 1649 and 1655 cm^{-1} matched with C═O vibrations, 1513 cm^{-1} is indicative of C stretching in polyphenols, 1412 cm^{-1} corresponds to C−C stretching in aromatic groups, 1338 and 1366 cm^{-1} indicate C−N stretch of aromatic amines, and 1021 and 1055 cm^{-1} match with the C−O stretching mode of esters.[59] The absorption region at 902 and 942 cm^{-1} can be assigned to HO−C═O stretching bands.[60] The tetrahedral coordination of Zn is revealed by the peaks at 840 and 845 cm^{-1}.[61] The peak at 721 and 772 cm^{-1} implies the presence of a metal oxide bond. The Zn−O bond is allotted to the bands at 648 and 670 cm^{-1}. The FTIR results of the leaf extract (Figure 3c) demonstrated the presence of the functional groups of biomolecules that were responsible for the reduction of the metal precursor to the desired products. A broad band at 3273 cm^{-1} matched with the O−H stretching of phenols and N−H stretching of amides, while the weak band at 2969 cm^{-1} is associated with the C−H bend of the aldehydic group. The absorbance at 1570 cm^{-1} is due to the asymmetric C═O stretching of the carboxylate group.[62] The vibrational band at 1406 cm^{-1} corresponds to $-NH_2$ of flavonoids and amines,[63] while the broad strong peak at 1027 cm^{-1} is associated with the C═O amide band of the aliphatic carboxylic acid group.[42] The inferences thus point to the presence of phenols, flavonoids, primary amines, and amino acids in the leaf extract.

https://doi.org/10.1021/acsomega.2c07530
ACS Omega 2023, 8, 10954−10967

3.4. XRD. Phase purity, average crystallite size, and crystallinity of ZPCB and ZPB were examined by XRD, the spectra of which are shown in Figure 4. The XRD peaks were

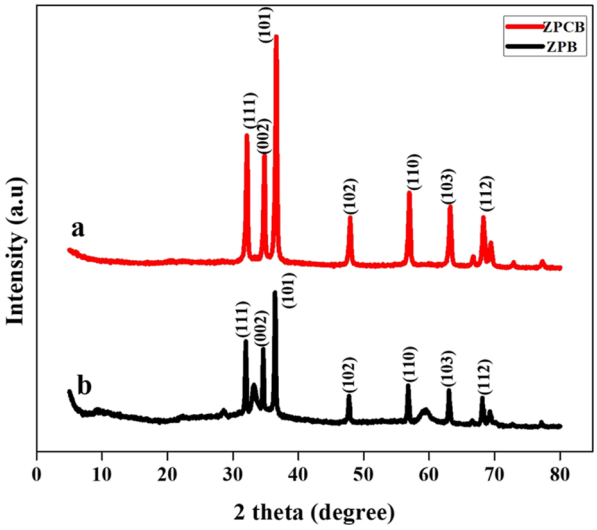

Figure 4. XRD pattern of (a) ZPCB and (b) ZPB.

sharp, indicating that the NPs are in good crystalline form. The XRD patterns of ZPCB demonstrated some unique diffraction peaks situated at 2θ values of 32.1, 34.8, 36.5, 47.8, 56.9, 63.1, and 68.3° which could be indexed to (111), (002), (101), (102), (110), (103), and (112), respectively. For ZPB, the peaks were observed at 2θ = 32, 34.8, 36.4, 47.7, 56.9, 63.1, and 68.1° corresponding to (111), (002), (101), (102), (110), (103), and (112), respectively. These patterns point to the hexagonal wurtzite structure of the pure phase with highly crystalline peaks. The values too corresponded well with JCPDS card no. 00-013-0311. The crystallite size of ZPCB was 17.9 nm, while ZPB had an average crystallite size of 19.4 nm which was calculated with the help of the Debye Scherrer equation given by pure-phase monoclinic crystalline morphology

$$D = \frac{0.9\lambda}{\beta \cos\theta} \quad (4)$$

Here, D is the crystallite size, λ is the wavelength of the X-ray sources whose value is 0.15406 nm, β is the full width at half-maximum in radians, and θ is the Bragg diffraction angle in degrees.

3.5. FESEM with EDAX. FESEM helped in investigating the surface morphology and structure of the NPs whose corresponding images are displayed in Figure 5a,b. The images display rodlike and semispherical structures for both ZPCB and ZPB.

The qualitative and quantitative analyses of the samples was carried out with the help of EDAX analysis, the results of which can be observed in Figure 5c,d. The presence of Zn and O as elemental compositions was confirmed by EDAX results. In ZPCB, the weight percentage of Zn was 68.94% and that of O was 15.82%. The 15.25% of C observed in ZPCB could be due to the use of chitosan and plant extract. In ZPB, the weight percentage of Zn was 62.98, while O had 37.61%. Beside the Zn and O peaks, some unknown peaks are observed at around 2.00 and 3.8 keV. These peaks may be due to different elements present in the plant extract.

3.6. HRTEM with SAED. The synthesized NPs' size and morphology were evaluated by HRTEM as shown in Figure 6a,b. The images confirmed the rodlike and semispherical structure of the NPs as seen in SEM. In ZPCB, some hexagonal shapes are also observed. Rod-shaped and hexagonal ZnO NPs are reported by Velsankar et al. Spherical and hexagonal-shaped ZnO NPs are found in the literature (refs 58, 64, and 65). The efficacy of the NPs in various applications depends much on their morphology and size.

The bright circular spots in the SAED patterns observed in Figure 6c,d give us information regarding the polycrystalline nature of the NPs. The *d*-spacing values for ZPCB were 0.23 and 0.29 nm, coinciding with the XRD pattern, and were assigned the hkl values of (002) and (101), respectively. The *d*-spacing values for ZPB were 0.28, 0.26, and 0.24 nm which agrees well with the XRD value of '*d*,' confirming the hexagonal wurtzite structure of the ZnO NPs. The concentric rings were assigned the values of (111), (002), and (101) in agreement with XRD findings.

Figure 6e,f displays the histogram of the particle size. The size of ZPCB ranged from 25 to 60 nm with 43 nm as the average size. ZPB's size ranged from 20 to 70 nm and had an average size of 45 nm. The small-sized NPs bearing the advantage of possessing a larger surface area are of greater advantage in terms of their various applications.

3.7. Antidiabetic Potential. The nanomedicine approach which could be an effective alternative to insulin in treating diabetes is gaining ground in the field of research. Studies of previous works of literature show that ZnO is known to possess antidiabetic properties.[17,50,66] Constraining the activity of α-amylase aids in reducing the glucose absorption rate as the enzyme plays a vital role in hydrolyzing carbohydrates. The present study on the role of the synthesized ZnO NPs as potential α-amylase inhibitors revealed that they are good antidiabetic agents. Figure 7 and Table 1 show the percentage of inhibition profile of ZPCB and ZPB for α-amylase activity. The highest activity was noticed in ZPCB with 74% inhibition at the highest concentration and having an IC_{50} value of 14.46 μg/mL. The synergistic effect of chitosan and biomolecules from the leaf extract is credited with ZPCB having a higher inhibitory effect. It is also observed that at lower concentrations, the inhibitory potential of ZPCB is even higher than that of acarbose which was used as the standard. ZPB too exhibited good antidiabetic efficiency with 72% inhibition, and its IC_{50} value was 17.51 μg/mL. From the results, it is evident that the inhibitory activity increases with an increase in the concentration of NPs and vice versa.

3.8. Antioxidant Potential. Reactive oxygen species (ROS) which are highly reactive are produced during the mitochondrial oxidative metabolism.[67] An excess of ROS leads to oxidative stress that results in cellular damage or abnormal cell growth. Antioxidants, therefore, help in preventing or reducing ROS-induced oxidative damage either by reacting directly with free radicals or by constraining the activities of the free radical-generating enzymes.[68]

DPPH, a stable free radical, has an absorbance between 512 and 520 nm in its oxidized state. DPPH can accept an electron or hydrogen radical to form a stable diamagnetic molecule. A shift in color from purple to yellow denotes a decrease in the absorbance of the DPPH radical which ultimately demonstrates that the antioxidant material interacted with the free radical. In this method, antioxidants present in the sample reduce the stable nitrogen radical in DPPH, leading to a drop in the absorbance.

https://doi.org/10.1021/acsomega.2c07530
ACS Omega 2023, 8, 10954−10967

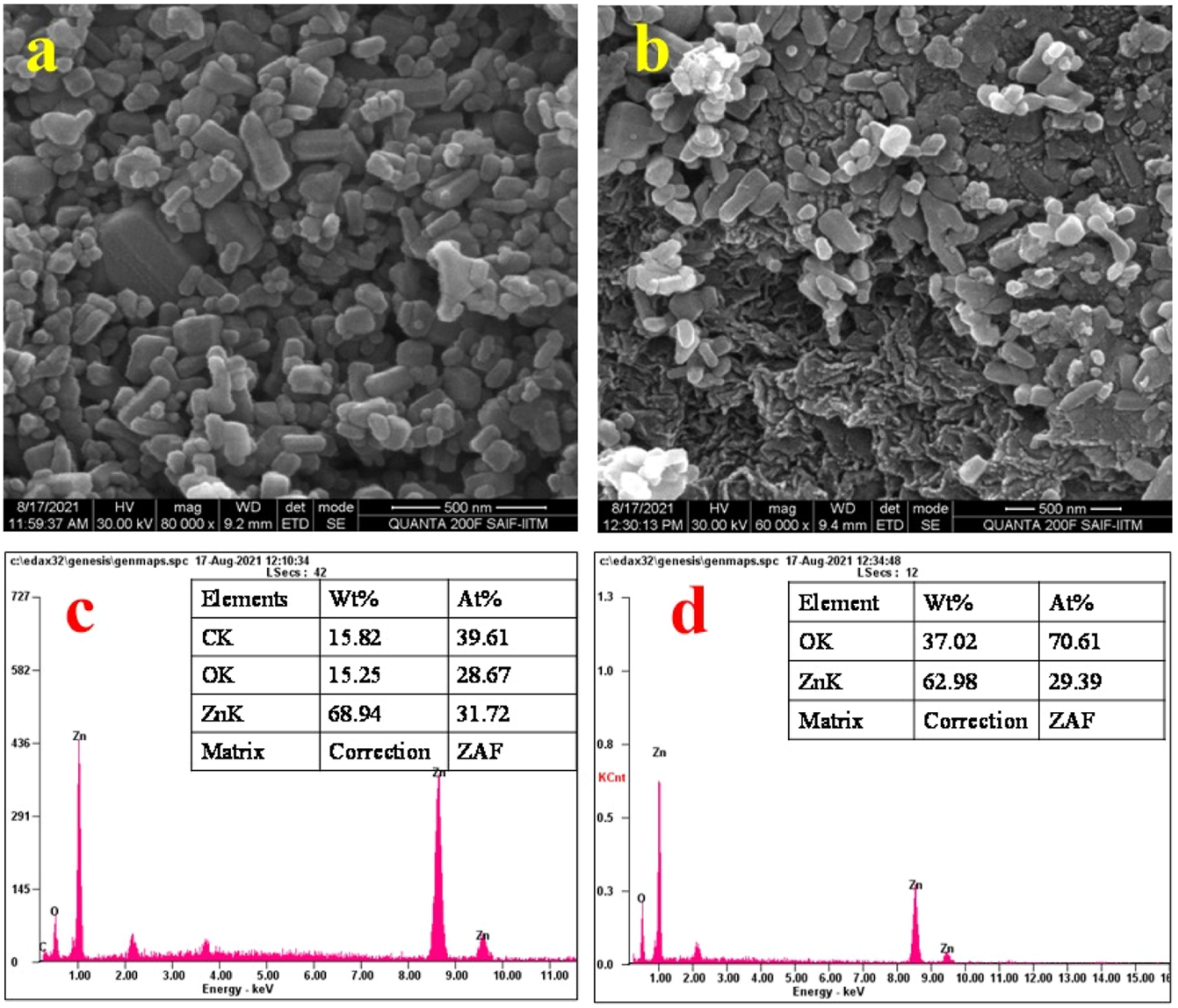

Figure 5. FESEM images of (a) ZPCB and (b) ZPB. EDAX of (c) ZPCB and (d) ZPB.

In the present work, the antioxidant potential of the biosynthesized ZnO NPs was assessed by the in vitro DPPH radical scavenging assay. The results as observed in Figure 8 and Table 2 indicate that with an increase in the NP concentration, their effectiveness too increased. In ZPCB, a gradual increase in the inhibitory percentage is noticed, reaching a maximum of 78% at its highest concentration, while in ZPB, a sudden leap in their activity is observed on reaching 800 μg/mL. ZnO NPs transfer their electron density toward the free radical which is situated at the nitrogen atom in DPPH.[69] Similar reports on the effective antioxidant property of ZnO NPs are reported in the literature (Table 3).[70−72]

3.9. Cytotoxicity. Cell morphological variations such as retardation of cell growth or cell ruptures were studied to investigate the cytotoxic nature of the NPs. The in vitro cytotoxic potential of ZnO NPs was performed against MG-63 human osteosarcoma cells, and the viability of the cells was studied using the MTT assay. On exposure to the NPs, there was a noticeable reduction in cell viability in a dose-dependent manner. The IC_{50} value which was calculated by employing the linear regression equation was found to be 62.61 μg/mL. At the highest concentration (500 μg/mL), the percentage of cell viability was found to be 10.65%. Figure 9 shows the images of negative control cells and ZPCB-treated cells at different concentrations, whereby one can notice the change in morphology as well as the reduction in terms of cell viability.

The known mechanisms involved in the cytotoxicity of nanomaterials are physical direct interaction of extremely sharp edges of nanomaterials with the cell wall membrane,[73] ROS generation[74] even in the dark,[75] trapping the cells within the aggregated nanomaterials for bacteria[76] and for spermatozoa,[77] oxidative stress,[78] DNA damaging and chromosomal aberration,[79] Zn ion release,[80] neuronal[81] and hormonal[82] side effects, and contribution in generation/explosion of nanobubbles.[83] A mechanism proposed for the cytotoxic effect in our current work is the production of ROS which in turn leads to cellular damage and thereby apoptosis. The generation of ROS by metal oxide NPs is due to their semiconductor nature by which electrons and holes are generated. These electrons and holes, in turn, interact with oxygen and hydroxyl ions, thereby resulting in extremely reactive free radicals which are responsible for oxidative damage to cells.[84]

https://doi.org/10.1021/acsomega.2c07530
ACS Omega 2023, 8, 10954−10967

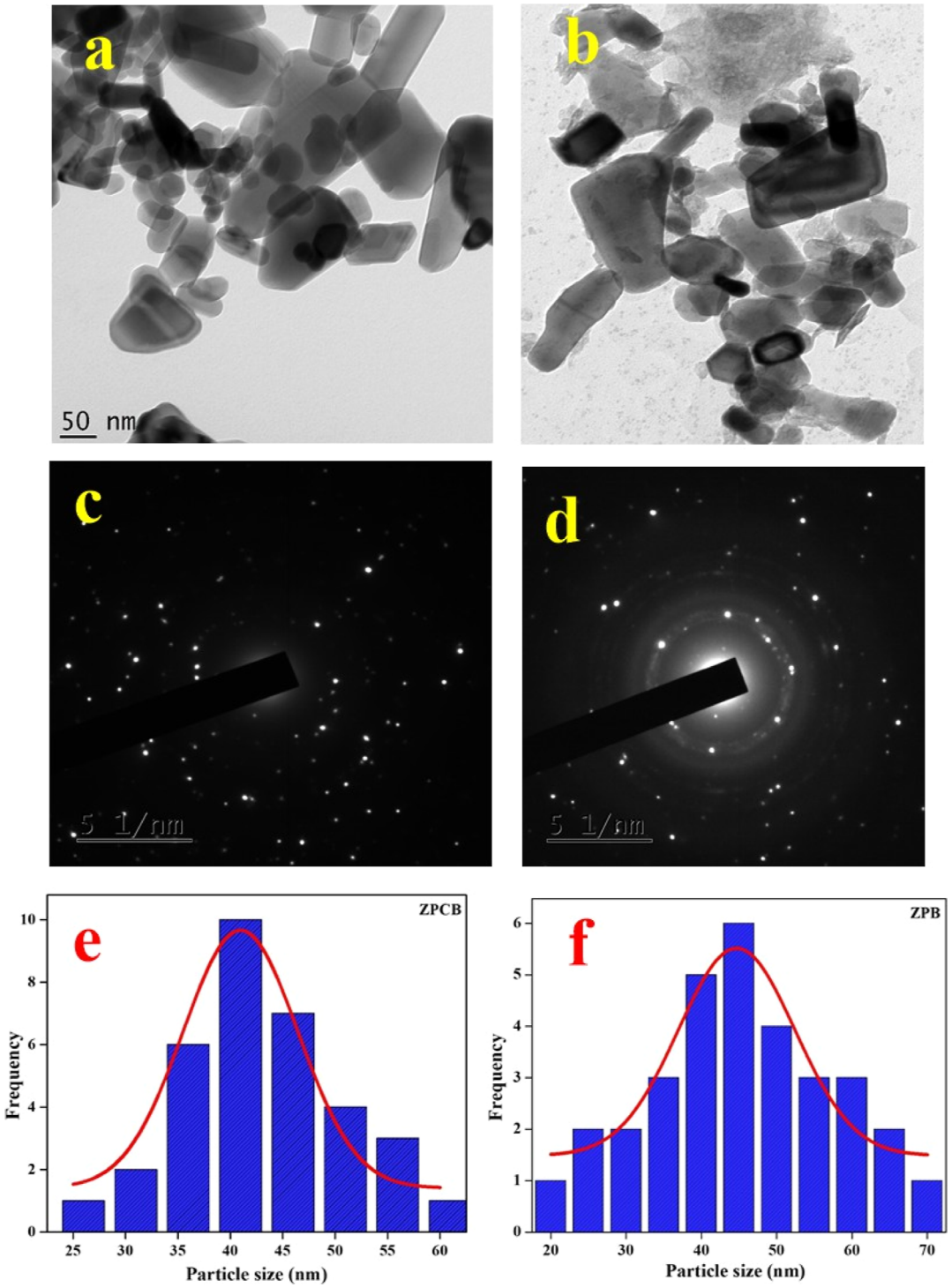

Figure 6. HRTEM images of (a) ZPCB and (b) ZPB. SAED images of (c) ZPCB and (d) ZPB. Histogram of particle size of (e) ZPCB and (f) ZPB.

3.10. Photocatalytic Potential. The photocatalytic potential of biosynthesized ZnO NPs was investigated using two factors: dye concentration and contact time. Decolorization of the dye indicated its degradation, and the associated absorbance was recorded with the help of a UV−vis spectrophotometer. The dose-dependent outcome is evident as the percentage of dye degradation increased with an increase in the concentration and contact time (Figure 10). In the graph, the lighter shade represents the concentration of the dye, while the darker shade denotes the percentage of dye degradation. It is clear from the graph that as the concentration of the NPs and the exposed time duration increased, dye degradation increased, while the dye concentration decreased. A maximum of 91% of dye was degraded in the presence of ZPCB with an IC_{50} value of 26.36 μg/mL, while for ZCB, the maximum percentage of dye degradation was 84% and the IC_{50} value was 33.90 μg/mL. ZPCB, being slightly smaller in size, had better photocatalytic efficiency. The smaller NPs have the advantage of quicker photocatalytic reaction due to the larger surface area.

https://doi.org/10.1021/acsomega.2c07530
ACS Omega 2023, 8, 10954−10967

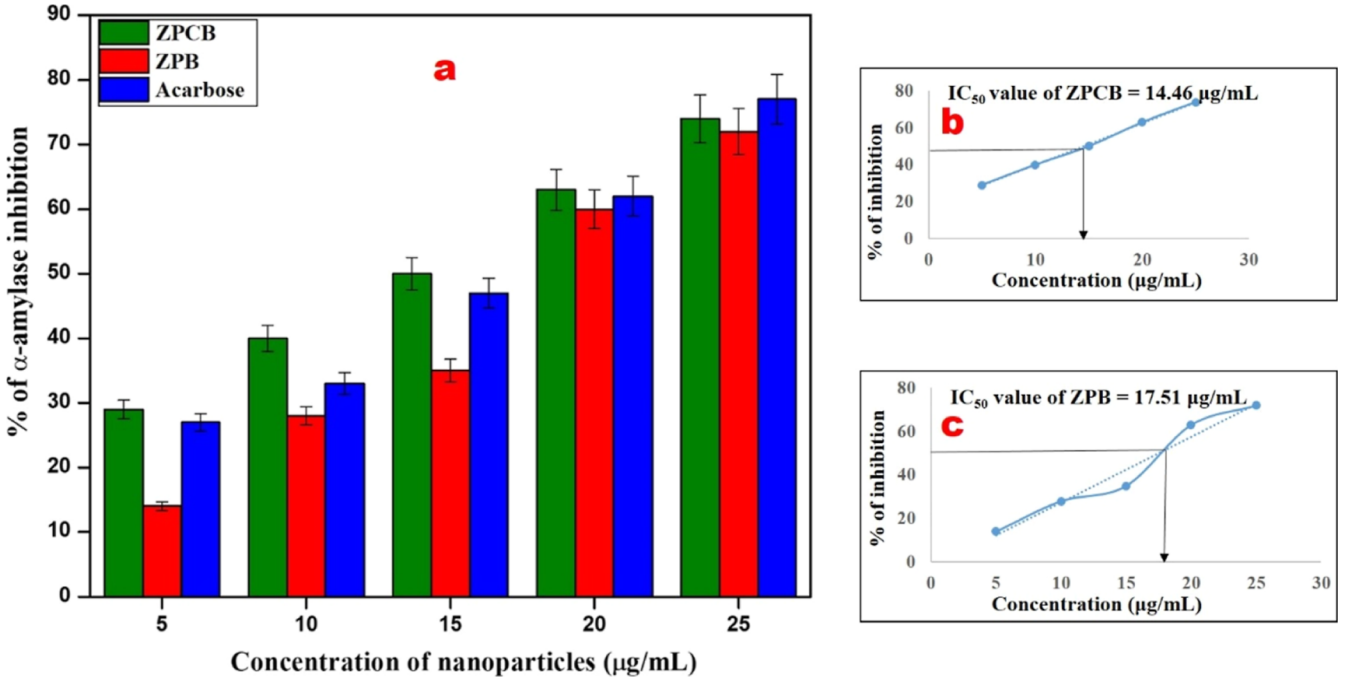

Figure 7. (a) Antidiabetic activities of ZPCB, ZPB, and standard (acarbose). (b,c) Linear regression graph to determine IC_{50} values of ZPCB and ZPB, respectively. The results are denoted as means ± standard error (SE) of the mean, and the error bar size reveals the sample variation of triplicates.

Table 1. α-Amylase Inhibition Activity of Acarbose, ZPCB, and ZPB at Different Concentrations

concentration (μg/mL)	(std.) acarbose (%)	ZPCB (%)	ZPB (%)
5	27 ± 0.35	29 ± 0.47	14 ± 0.70
10	33 ± 0.65	40 ± 1.12	28 ± 0.42
15	47 ± 1.35	50 ± 1.52	35 ± 0.75
20	62 ± 2.11	63 ± 2.15	60 ± 2.10
25	77 ± 2.83	74 ± 2.71	72 ± 2.60

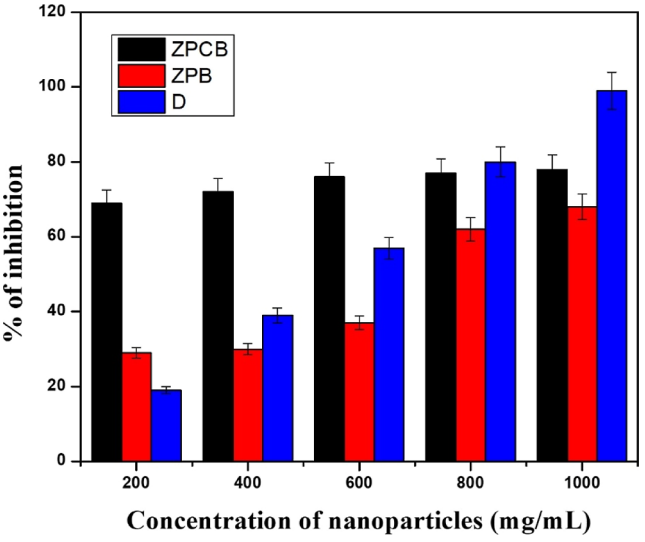

Figure 8. Antioxidant activities of ZPCB, ZPB, and standard (ascorbic acid). The results are denoted as means ± SE of the mean, and the error bar size reveals the sample variation of triplicates with the statistical significance at $p < 0.05$.

Table 2. DPPH Radical Scavenging Activity of Ascorbic Acid (Standard), ZPCB, and ZPB at Different Concentrations

concentration (μg/mL)	(std.) ascorbic acid (%)	ZPCB (%)	ZPB (%)
200	19 ± 0.75	69 ± 1.45	29 ± 0.45
400	39 ± 0.95	72 ± 1.60	30 ± 0.51
600	57 ± 1.32	76 ± 1.86	37 ± 0.85
800	81 ± 2.10	77 ± 1.73	62 ± 1.33
1000	>99 ± 2.73	78 ± 1.90	68 ± 1.40

Table 3. Photocatalytic Efficiency of ZPCB and ZPB

(i) at varied concentration				
	% of dye degradation		concentration of dye (μg/mL)	
concentration of ZnO NPs (μg)	ZPCB	ZPB	ZPCB	ZPB
0	0	0	100 ± 3.20	100 ± 3.18
10	21 ± 0.05	6 ± 0.30	78 ± 2.74	93 ± 3.35
20	38 ± 0.90	19 ± 0.75	61 ± 2.05	80 ± 3.01
30	60 ± 2.12	34 ± 0.97	39 ± 0.75	65 ± 2.25
40	75 ± 2.71	64 ± 2.23	24 ± 0.22	35 ± 0.76
50	91 ± 3.19	86 ± 3.21	8 ± 0.14	13 ± 0.72
(ii) at varied time.				
	% of dye degradation		concentration of dye (μg/mL)	
time (h)	ZPCB	ZPB	ZPCB	ZPB
0	0	0	100 ± 3.12	100 ± 3.15
2	16 ± 0.80	8 ± 0.40	83 ± 3.12	91 ± 3.05
4	36 ± 0.96	14 ± 0.71	63 ± 2.27	82 ± 2.91
6	59 ± 1.87	34 ± 0.76	40 ± 1.06	67 ± 2.35
8	77 ± 2.85	57 ± 1.85	22 ± 1.19	40 ± 1.06
10	88 ± 3.40	84 ± 3.06	9 ± 0.45	13 ± 0.65

On light irradiation of the particles, the valence band electrons get excited and jump to the conduction band, creating an equal number of electrons (e^-_{cb}) and holes (h^+_{vb}). The e^-_{cb}, on reacting with molecular oxygen yield $O_2^{\bullet}$ which further react with H^+ and form $HO_2^{\bullet}$, finally converting into H_2O_2 and O_2.

https://doi.org/10.1021/acsomega.2c07530
ACS Omega 2023, 8, 10954−10967

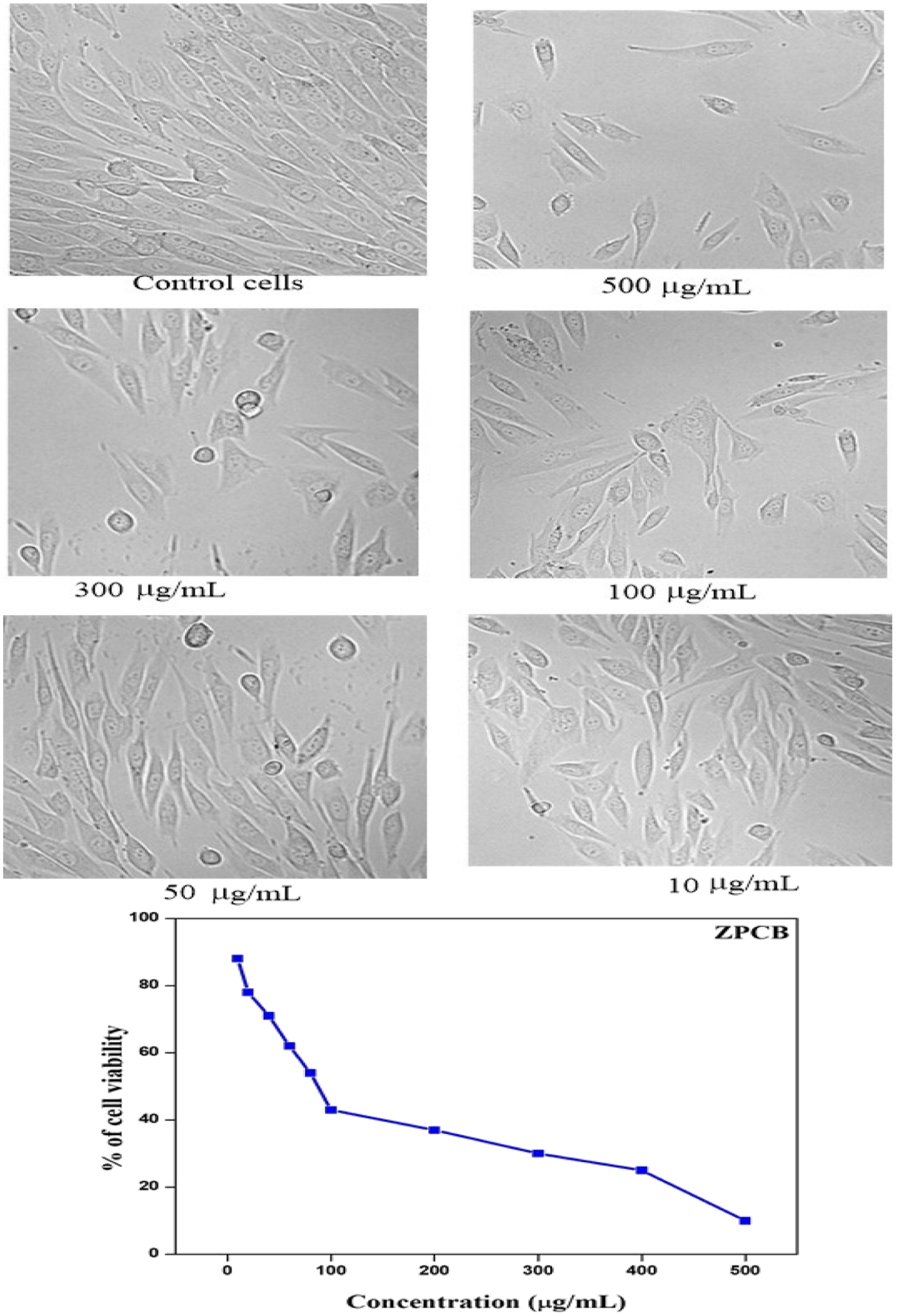

Figure 9. Images showing the negative control cells and ZPCB-treated cells at different concentrations.

H_2O_2, in the presence of light, produces $OH^{\bullet}$. The h^{+}_{vb} too react with water, forming H^{+} and $OH^{\bullet}$. These generated reactive species are strong oxidizing agents, responsible for oxidizing the dye and degrading them.[85] The green-synthesized ZnO NPs can

https://doi.org/10.1021/acsomega.2c07530
ACS Omega 2023, 8, 10954−10967

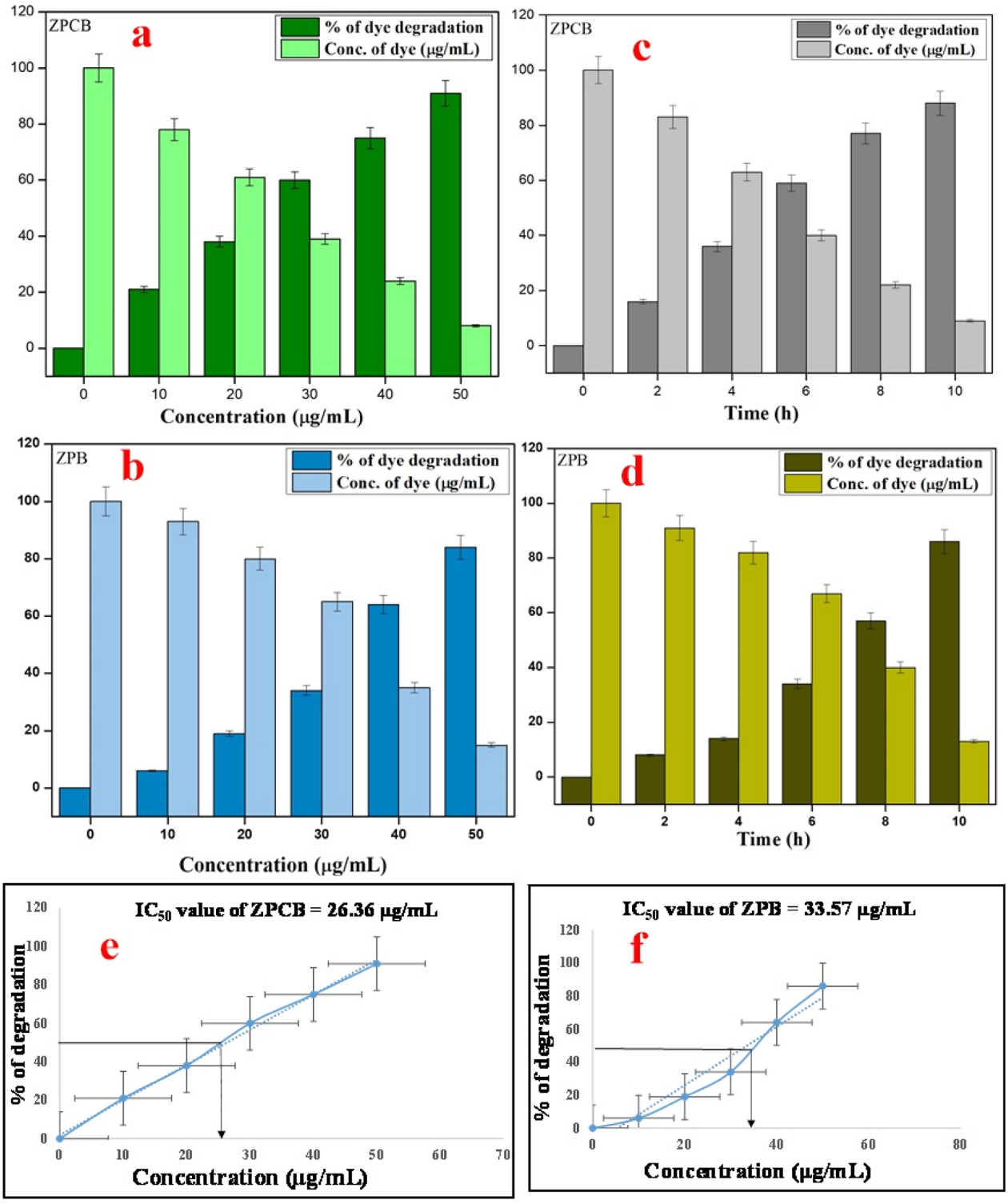

Figure 10. Photocatalytic activity of ZPCB and ZPB at (a ,b) different concentrations and (c,d) at different times. (e,f) Linear regression graph to determine the IC_{50} values of ZPCB and ZPB.

thus serve as an agent to address environmental issues, especially those that pertain to pollution, arising out of the use of dye. ZnO NPs, as a potential candidate for dye degradation, have been reported in previous findings too[86−88]

4. CONCLUSIONS

ZnO NPs were synthesized by the biogenic method, and a comparative study between the ZnO NPs fabricated through the mediation of chitosan and aqueous leaf extract of *E. blanda* (ZPCB) and mediation of leaf extract alone (ZPB) was carried out. ZPCB was found to be more effective in all activities that were carried out—antidiabetic, antioxidant, cytotoxic, and photocatalytic. The higher efficiency is attributed to the synergistic effect of chitosan and biomolecules found in the leaf extract. The study concludes that the green synthesis of NPs bears the greater advantage of easy availability, time, and cost-

https://doi.org/10.1021/acsomega.2c07530
ACS Omega 2023, 8, 10954−10967

effectiveness and is environmentally benign. The results of the various tests prove that the biosynthesized ZnO NPs could be effectively used for various biomedical applications and also for the treatment of contaminated wastewater.

The limitation of our work lies in carrying out all biological activities in vitro. Hence, the future scope of our research work includes the following:

- In vivo studies of biological activities to prove biomedical applications.
- Testing for the degradation of more dyes and other pollutants which could serve as potential precursors for environmental remediation.

AUTHOR INFORMATION

Corresponding Authors

Augustine Arul Prasad T − *PG and Research Department of Chemistry, Dwarakadoss Goverdhandoss Vaishnav College (Autonomous) (Affiliated to University of Madras), Chennai 600106, India*; Phone: +91-9444278265; Email: augustineap@gmail.com

Tamizhdurai Perumal − *PG and Research Department of Chemistry, Dwarakadoss Goverdhandoss Vaishnav College (Autonomous) (Affiliated to University of Madras), Chennai 600106, India*; orcid.org/0000-0002-7955-7287; Phone: +91-9677146579; Email: tamizhvkt2010@gmail.com

Mani Govindasamy − *Faculty, International Ph.D. Program in Innovative Technology of Biomedical Engineering and Medical Devices, Ming Chi University of Technology, New Taipei City 243303, Taiwan; Adjunct Faculty, Department of Research and Innovation, Saveetha School of Engineering, SIMATS, Chennai 602105, India; Korea University of Technology and Education, Cheonan-si 31253 Chungcheongnam-do, Republic of Korea*; Phone: +886-989419993; Email: govindasamy420700@gmail.com

Authors

Athisa Roselyn Maheo − *PG and Research Department of Chemistry, Auxilium College (Autonomous) (Affiliated to Thiruvalluvar University, Serkadu), Vellore 632006, India*

Scholastica Mary Vithiya B − *PG and Research Department of Chemistry, Auxilium College (Autonomous) (Affiliated to Thiruvalluvar University, Serkadu), Vellore 632006, India*

V. L. Mangesh − *Department of Mechanical Engineering, Koneru Lakshmaiah Education Foundation, Guntur 522502 Andhra Pradesh, India*; orcid.org/0000-0003-0996-9822

Wahidah H. Al-Qahtani − *Department of Food Sciences & Nutrition, College of Food & Agriculture Sciences, King Saud University, Riyadh 11451, Saudi Arabia*

Complete contact information is available at: https://pubs.acs.org/10.1021/acsomega.2c07530

Author Contributions

CRediT authorship contribution statement: **Athisa Roselyn Maheo:** Visualization, investigation, and writing; **B. Scholastica Mary Vithiya:** Visualization and investigation. **T. Augustine Arul Prasad:** Review & editing; **Wahidah H. Al-Qahtani**: Project administration, funding acquisition; and **Mani Govindasamy**: Conceptualization, investigation, investigation methodology, review and editing.

Notes

The authors declare no competing financial interest.

ACKNOWLEDGMENTS

This work was funded by the Researchers Supporting Project number (RSP2023R293) King Saud University, Riyadh, Saudi Arabia. This work was funded by the Ming Chi University of Technology, Taiwan. The authors are grateful to the Auxilium College (Autonomous), Vellore and Vellore Institute of Technology, Vellore, India, for providing lab facilities for the research.

REFERENCES

(1) Jiang, M.; Han, T.; Zhang, X. Hollow C@ SnS_2/SnS Nanocomposites : High Efficient Oxygen Evolution Reaction Catalysts. *J. Colloid Interface Sci.* **2021**, *583*, 149−156.

(2) Dai, T.; Wan, Y.; Tian, R.; Wang, S.; Han, T.; Wang, G. In Situ Cation Exchange Generated ZnS − Ag_2S Nanoparticles for Photothermal Detection of Transcription Factor. *ACS Appl. Bio Mater.* **2020**, *3*, 3260−3267.

(3) Das, S.; Mukhopadhyay, S.; Chatterjee, S.; Devi, P. S.; Suresh Kumar, G. Fluorescent ZnO-Au Nanocomposite as a Probe for Elucidating Specificity in DNA Interaction. *ACS Omega* **2018**, *3*, 7494−7507.

(4) Veisi, H.; Mohammadi, L.; Hemmati, S.; Tamoradi, T.; Mohammadi, P. In Situ Immobilized Silver Nanoparticles on Rubia Tinctorum Extract- Coated Ultrasmall Iron Oxide Nanoparticles: An Efficient Nanocatalyst with Magnetic Recyclability for Synthesis of Propargylamines by A^3 Coupling Reaction. *ACS Omega* **2019**, *4*, 13991−14003.

(5) Agarwal, H.; Venkat Kumar, S.; Rajeshkumar, S. A Review on Green Synthesis of Zinc Oxide Nanoparticles − An Eco-Friendly Approach. *Resour. Technol.* **2017**, *3*, 406−413.

(6) Álvarez-Chimal, R.; García-Pérez, V. I.; Álvarez-Pérez, M. A.; Tavera-Hernández, R.; Reyes-Carmona, L.; Martínez-Hernández, M.; Arenas-Alatorre, J. A. Influence of the Particle Size on the Antibacterial Activity of Green Synthesized Zinc Oxide Nanoparticles Using Dysphania Ambrosioides Extract , Supported by Molecular Docking Analysis. *Arabian J. Chem.* **2022**, *15*, 103804.

(7) Sabeena, G.; Rajaduraipandian, S.; Pushpalakshmi, E.; Alhadlaq, H. A.; Mohan, R.; G, G.; Ahamed, M. Green and Chemical Synthesis of CuO Nanoparticles: A Comparative Study for Several in Vitro Bioactivities and in Vivo Toxicity in Zebrafish Embryos. *J. King Saud Univ., Sci.* **2022**, *34*, 102092.

(8) Vinodhini, S.; Vithiya, B. S. M.; Prasad, T. A. A. Green Synthesis of Palladium Nanoparticles Using Aqueous Plant Extracts and Its Biomedical Applications. *J. King Saud Univ., Sci.* **2022**, *34*, 102017.

(9) Vinodhini, S.; Vithiya, B. S. M.; Prasad, T. A. A. Synthesis and Characterization of Palladium Nanoparticles Using Leaf Extracts. *Ann. Romanian Soc. Cell Biol.* **2021**, *25*, 913−923.

(10) Thomas, B.; Vithiya, T. A. A.; Prasad, B. S. M.; Mohamed, S. B.; Magdalane, C. M.; Kaviyarasu, K.; Maaza, M. Antioxidant and Photocatalytic Activity of Aqueous Leaf Extract Mediated Green Synthesis of Silver Nanoparticles Using Passiflora Edulis f. Flavicarpa. *J. Nanosci. Nanotechnol.* **2019**, *19*, 2640−2648.

(11) Maheo, A. R.; B, S. M. V.; T, A. A. P. Biosynthesis and Characterization of Eupatorium Adenophorum and Chitosan Mediated Copper Oxide Nanoparticles and Their Antibacterial Activity. *Results Surfaces and Interfaces* **2022**, *6*, 100048.

(12) Maheo, A. R.; Vithiya, B. S. M.; Prasad, T. A. A.; Tamizhdurai, P.; Mangesh, V. L. Biosynthesis, Characterization, Biological and Photo Catalytic Investigations of Elsholtzia Blanda and Chitosan Mediated Copper Oxide Nanoparticles: Biosynthesis, Characterization, Biological and Photo Catalytic Investigations. *Arabian J. Chem.* **2022**, *15*, 103661.

(13) Jacob, J.; Prasad, T. A. A.; Vithiya, B. S. M.; Athisa, M. R. Biosynthesis of Bimetallic Cu-Ag Nanocomposites and Evaluation of Their Electrocatalytic, Antibacterial and Anti-Cancerous Activity. *J. Appl. Chem.* **2022**, *16*, 955−966.

https://doi.org/10.1021/acsomega.2c07530
ACS Omega 2023, 8, 10954−10967

(14) Akhavan, O.; Ghaderi, E.; Abouei, E.; Hatamie, S.; Ghasemi, E. Accelerated Differentiation of Neural Stem Cells into Neurons on Ginseng-Reduced Graphene Oxide Sheets. *Carbon* **2014**, *66*, 395−406.
(15) Alhalili, Z. Green Synthesis of Copper Oxide Nanoparticles CuO NPs from Eucalyptus Globoulus Leaf Extract : Adsorption and Design of Experiments. *Arabian J. Chem.* **2022**, *15*, 103739.
(16) Vijayakumar, N.; Bhuvaneshwari, V.; Ayyadurai, G.; Jayaprakash, R.; Gopinath, K.; Nicoletti, M.; Alarifi, S.; Govindarajan, M. Green Synthesis of Zinc Oxide Nanoparticles Using Anoectochilus Elatus, and Their Biomedical Applications. *Saudi J. Biol. Sci.* **2022**, *29*, 2270−2279.
(17) Faisal, S.; Jan, H.; Shah, S. A.; Shah, S.; Khan, A.; Akbar, M. T.; Rizwan, M.; Jan, F.; Wajidullah; Akhtar, N.; Khattak, A.; Syed, S. Green Synthesis of Zinc Oxide (ZnO) Nanoparticles Using Aqueous Fruit Extracts of Myristica Fragrans: Their Characterizations and Biological and Environmental Applications. *ACS Omega* **2021**, *6*, 9709−9722.
(18) Akhavan, O.; Ghaderi, E. Cu and CuO Nanoparticles Immobilized by Silica Thin Films as Antibacterial Materials and Photocatalysts. *Surf. Coat. Technol.* **2010**, *205*, 219−223.
(19) Cai, X.; Zhu, Q.; Zeng, Y.; Zeng, Q.; Chen, X.; Zhan, Y. Manganese Oxide Nanoparticles As MRI Contrast Agents In Tumor Multimodal Imaging And Therapy. *Int. J. Nanomed.* **2019**, *14*, 8321−8344.
(20) Akhavan, O.; Ghaderi, E. Flash Photo Stimulation of Human Neural Stem Cells on Graphene/TiO_2 Heterojunction for Differentiation into Neurons. *Nanoscale* **2013**, *5*, 10316−10326.
(21) Treccani, L.; Maiwald, M.; Zöllmer, V.; Busse, M.; Grathwohl, G.; Rezwan, K. Antibacterial and Abrasion-Resistant Alumina Micropatterns. *Adv. Eng. Mater.* **2009**, *11*, B61−B66.
(22) Quan, Q.; Xie, J.; Gao, H.; Yang, M.; Zhang, F.; Liu, G.; Lin, X.; Wang, A.; Eden, H. S.; Lee, S.; et al. HSA Coated Iron Oxide Nanoparticles as Drug Delivery Vehicles for Cancer Therapy. *Mol. Pharm.* **2011**, *8*, 1669−1676.
(23) Charbgoo, F.; Ahmad, M. B.; Darroudi, M. Cerium Oxide Nanoparticles: Green Synthesis and Biological applications. *Int. J. Nanomed.* **2017**, *12*, 1401−1413.
(24) Roy, A.; Srivastava, S. K.; Shrivastava, S. L.; Mandal, A. K. Hierarchical Assembly of Nanodimensional Silver−Silver Oxide Physical Gels Controlling Nosocomial Infections. *ACS Omega* **2020**, *5*, 32617−32631.
(25) Ahmed, S.; Annu; Chaudhry, S. A.; Ikram, S. A Review on Biogenic Synthesis of ZnO Nanoparticles Using Plant Extracts and Microbes: A Prospect towards Green Chemistry. *J. Photochem. Photobiol., B* **2017**, *166*, 272−284.
(26) Barui, A. K.; Kotcherlakota, R.; Patra, C. R. Biomedical Applications of Zinc Oxide Nanoparticles. *Inorg. Frameworks Smart Nanomed.* **2018**, 239−278.
(27) Rabiee, N.; Akhavan, O.; Fatahi, Y.; Mohammad, A.; et al. CaZnO-Based Nanoghosts for the Detection of SsDNA , PCRISPR and Recombinant SARS-CoV-2 Spike Antigen and Targeted Delivery of Doxorubicin. *Chemosphere* **2022**, *306*, 135578.
(28) Rajabi, H. R.; Naghiha, R.; Kheirizadeh, M.; Sadatfaraji, H.; Mirzaei, A.; Alvand, Z. M. Microwave Assisted Extraction as an Efficient Approach for Biosynthesis of Zinc Oxide Nanoparticles : Synthesis , Characterization, and Biological Properties. *Mater. Sci. Eng. C* **2017**, *78*, 1109−1118.
(29) Ali, H. M.; Ibrahim, O. M.; Ali, A. S. M.; Mohamed, M. A.; Ghareeb, R. Y.; Hafez, E. E.; El-Aassar, M. R. Cross-Linked Chitosan / Gelatin Beads Loaded with Chlorella Vulgaris Microalgae/Zinc Oxide Nanoparticles for Adsorbing Carcinogenic Bisphenol - A Pollutant from Water. *ACS Omega* **2022**, *7*, 27239−27248.
(30) Devi, N. K.; Dutta, S.; Das, R.; Devi, A. S.; Devi, N. M.; Devi, K. S. Nephroprotective Effect Of Elsholtzia Blanda Benth . In Paracetamol Induced Toxicity In Albino Rats. *Int. J. Recent Sci. Res.* **2018**, *9*, 28186−28189.
(31) Lopez-Lazaro, M. Distribution and Biological Activities of the Flavonoid Luteolin. *Mini-Rev. Med. Chem.* **2009**, *9*, 31−59.
(32) Guo, Z.; Liu, Z.; Wang, X.; Liu, W.; Jiang, R.; Cheng, R.; She, G. Elsholtzia: Phytochemistry and Biological Activities. *Chem. Cent. J.* **2012**, *6*, 147.
(33) Kalaivani, R.; Maruthupandy, M.; Muneeswaran, T.; Hameedha Beevi, A. H.; Anand, M.; Ramakritinan, C. M.; Kumaraguru, A. K. Synthesis of Chitosan Mediated Silver Nanoparticles (Ag NPs) for Potential Antimicrobial Applications. *Front. Lab. Med.* **2018**, *2*, 30−35.
(34) Katas, H.; Moden, N. Z.; Lim, C. S.; Celesistinus, T.; Chan, J. Y.; Ganasan, P.; Suleman Ismail Abdalla, S.; Abdalla, I. Biosynthesis and Potential Applications of Silver and Gold Nanoparticles and Their Chitosan-Based Nanocomposites in Nanomedicine. *J. Nanotechnol.* **2018**, *2018*, 1−13.
(35) Leiva, A.; Bonardd, S.; Pino, M.; Saldías, C.; Kortaberria, G.; Radić, D. Improving the Performance of Chitosan in the Synthesis and Stabilization of Gold Nanoparticles. *Eur. Polym. J.* **2015**, *68*, 419−431.
(36) Shabaani, M.; Rahaiee, S.; Zare, M.; Jafari, S. M. Green Synthesis of ZnO Nanoparticles Using Loquat Seed Extract; Biological Functions and Photocatalytic Degradation Properties. *Lwt* **2020**, *134*, 110133.
(37) Pallela, P. N. V. K.; Ruddaraju, L. K.; Veerla, S. C.; Matangi, R.; Kollu, P.; Ummey, S.; Pammi, S. V. N. Synergetic Antibacterial Potential, Dye Degrading Capability and Biocompatibility of Asperagus Racemosus Root Assisted ZnO Nanoparticles. *Mater. Today Commun.* **2020**, *25*, 101574.
(38) Jayachandran, A.; T.R, T. R.; Nair, A. S. Green Synthesis and Characterization of Zinc Oxide Nanoparticles Using Cayratia Pedata Leaf Extract. *Biochem. Biophys. Rep.* **2021**, *26*, 100995.
(39) Ramesh, P.; Saravanan, K.; Manogar, P.; Johnson, J.; Vinoth, E.; Mayakannan, M. Green Synthesis and Characterization of Biocompatible Zinc Oxide Nanoparticles and Evaluation of Its Antibacterial Potential. *Sens. Bio-Sens. Res.* **2021**, *31*, 100399.
(40) Chakraborty, S.; Farida, J. J.; Simon, R.; Kasthuri, S.; Mary, N. L. Averrhoe Carrambola Fruit Extract Assisted Green Synthesis of Zno Nanoparticles for the Photodegradation of Congo Red Dye. *Surface. Interfac.* **2020**, *19*, 100488.
(41) Rajiv, P.; Rajeshwari, S.; Venckatesh, R. Bio-Fabrication of Zinc Oxide Nanoparticles Using Leaf Extract of Parthenium Hysterophorus L. and Its Size- Dependent Antifungal Activity against Plant Fungal Pathogens. *Spectrochim. Acta, Part A* **2013**, *112*, 384−387.
(42) Umar, H.; Kavaz, D.; Rizaner, N. Biosynthesis of Zinc Oxide Nanoparticles Using Albizia Lebbeck Stem Bark, and Evaluation of Its Antimicrobial, Antioxidant, and Cytotoxic Activities on Human Breast Cancer Cell Lines. *Int. J. Nanomed.* **2018**, *14*, 87−100.
(43) Rad, S. S.; Sani, A. M.; Mohseni, S. Biosynthesis, Characterization and Antimicrobial Activities of Zinc Oxide Nanoparticles from Leaf Extract of Mentha Pulegium (L.). *Microb. Pathog.* **2019**, *131*, 239−245.
(44) Fowsiya, J.; Madhumitha, G.; Al-Dhabi, N. A.; Arasu, M. V. Photocatalytic Degradation of Congo Red Using Carissa Edulis Extract Capped Zinc Oxide Nanoparticles. *J. Photochem. Photobiol., B* **2016**, *162*, 395−401.
(45) Fahimmunisha, B. A.; Ishwarya, R.; AlSalhi, M. S.; Devanesan, S.; Govindarajan, M.; Vaseeharan, B. Green Fabrication, Characterization and Antibacterial Potential of Zinc Oxide Nanoparticles Using Aloe Socotrina Leaf Extract: A Novel Drug Delivery Approach. *J. Drug Delivery Sci. Technol.* **2020**, *55*, 101465.
(46) Karthikeyan, C.; Sisubalan, N.; Sridevi, M.; Varaprasad, K.; Ghouse Basha, M. H.; Shucai, W.; Sadiku, R. Biocidal Chitosan-Magnesium Oxide Nanoparticles via a Green Precipitation Process. *J. Hazard. Mater.* **2021**, *411*, 124884.
(47) Zafar, N.; Uzair, B.; Niazi, M.; Sajjad, K.; Samin, S.; Arshed, G.; Rafiq, M. J.; Rafiq, S. Fabrication & Characterization of Chitosan Coated Biologically Synthesized TiO 2 Nanoparticles against PDR E. Coli of Veterinary Origin. *Adv. Polym. Technol.* **2020**, *2020*, 1−13.
(48) Revathi, T.; Thambidurai, S. Cytotoxic, Antioxidant and Antibacterial Activities of Copper Oxide Incorporated Chitosan-Neem Seed Biocomposites. *Int. J. Biol. Macromol.* **2019**, *139*, 867−878.
(49) Sivakamavalli, J.; Pandiselvi, K.; Park, K.; Kwak, I.-S. Garcinia Cambogia Assisted Synthesis of ZnO Nanoparticles Coupled with Chitosan for Antibacterial, Antibiofilm, Cytotoxic, Anticancer and Ecotoxicity Assessment. *J. Cluster Sci.* **2022**, *33*, 2249−2264.
(50) Prasad, A. R.; Basheer, S. M.; Williams, L.; Joseph, A. Highly Selective Inhibition of α-Glucosidase by Green Synthesised ZnO

https://doi.org/10.1021/acsomega.2c07530
ACS Omega 2023, 8, 10954−10967

Nanoparticles - In-Vitro Screening and in-Silico Docking Studies. *Int. J. Biol. Macromol.* **2019**, *139*, 712−718.
(51) Liu, Y. C.; Li, J. F.; Ahn, J. C.; Pu, J. Y.; Rupa, E. J.; Huo, Y.; Yang, D. C. Biosynthesis of Zinc Oxide Nanoparticles by One-Pot Green Synthesis Using Fruit Extract of Amomum Longiligulare and Its Activity as a Photocatalyst. *Optik* **2020**, *218*, 165245.
(52) Shamhari, N. M.; Wee, B. S.; Chin, S. F.; Kok, K. Y. Synthesis and Characterization of Zinc Oxide Nanoparticles with Small Particle Size Distribution. *Acta Chim. Slov.* **2018**, *65*, 578−585.
(53) Talam, S.; Karumuri, S. R.; Gunnam, N. Synthesis, Characterization, and Spectroscopic Properties of ZnO Nanoparticles. *ISRN Nanotechnol.* **2012**, *2012*, 1−6.
(54) Al-Ariki, S.; Yahya, N. A. A.; Al-A'nsi, S. A.; Jumali, M. H. H.; Jannah, A. N.; Abd-Shukor, R. Synthesis and Comparative Study on the Structural and Optical Properties of ZnO Doped with Ni and Ag Nanopowders Fabricated by Sol Gel Technique. *Sci. Rep.* **2021**, *11*, 11948.
(55) Gawade, V. V.; Gavade, N. L.; Shinde, H. M.; Babar, S. B.; Kadam, A. N.; Garadkar, K. M. Green Synthesis of ZnO Nanoparticles by Using Calotropis Procera Leaves for the Photodegradation of Methyl Orange. *J. Mater. Sci.: Mater. Electron.* **2017**, *28*, 14033−14039.
(56) Sheik Mydeen, S.; Raj Kumar, R.; Kottaisamy, M.; Vasantha, V. S. Biosynthesis of ZnO Nanoparticles through Extract from Prosopis Juliflora Plant Leaf: Antibacterial Activities and a New Approach by Rust-Induced Photocatalysis. *J. Saudi Chem. Soc.* **2020**, *24*, 393−406.
(57) Tabrizi Hafez Moghaddas, S. M.; Elahi, B.; Javanbakht, V. Biosynthesis of Pure Zinc Oxide Nanoparticles Using Quince Seed Mucilage for Photocatalytic Dye Degradation. *J. Alloys Compd.* **2020**, *821*, 153519.
(58) Vijayakumar, S.; Mahadevan, S.; Arulmozhi, P.; Sriram, S.; Praseetha, P. K. Green Synthesis of Zinc Oxide Nanoparticles Using Atalantia Monophylla Leaf Extracts: Characterization and Antimicrobial Analysis. *Mater. Sci. Semicond. Process.* **2018**, *82*, 39−45.
(59) Jafarirad, S.; Mehrabi, M.; Divband, B.; Kosari-Nasab, M. Biofabrication of Zinc Oxide Nanoparticles Using Fruit Extract of Rosa Canina and Their Toxic Potential against Bacteria: A Mechanistic Approach. *Mater. Sci. Eng. C* **2016**, *59*, 296−302.
(60) Matinise, N.; Fuku, X. G.; Kaviyarasu, K.; Mayedwa, N.; Maaza, M. ZnO Nanoparticles via Moringa Oleifera Green Synthesis: Physical Properties & Mechanism of Formation. *Appl. Surf. Sci.* **2017**, *406*, 339−347.
(61) Rajendrachari, S.; Taslimi, P.; Karaoglanli, A.; Uzun, O.; Alp, E.; Jayaprakash, G. K. Photocatalytic Degradation of Rhodamine B (RhB) Dye in Waste Water and Enzymatic Inhibition Study Using Cauliflower Shaped ZnO Nanoparticles Synthesized by a Novel One-Pot Green Synthesis Method. *Arabian J. Chem.* **2021**, *14*, 103180.
(62) Obeizi, Z.; Benbouzid, H.; Ouchenane, S.; Yılmaz, D.; Culha, M.; Bououdina, M. Biosynthesis of Zinc Oxide Nanoparticles from Essential Oil of Eucalyptus Globulus with Antimicrobial and Anti-Biofilm Activities. *Mater. Today Commun.* **2020**, *25*, 101553.
(63) Omidi, S.; Sedaghat, S.; Tahvildari, K.; Derakhshi, P.; Motiee, F. Biosynthesis of Silver Nanoparticles with Adiantum Capillus-Veneris l Leaf Extract in the Batch Process and Assessment of Antibacterial Activity. *Green Chem. Lett. Rev.* **2018**, *11*, 544−551.
(64) Vijayakumar, S.; Arulmozhi, P.; Kumar, N.; Sakthivel, B.; Prathip Kumar, S.; Praseetha, P. K. Acalypha Fruticosa L. Leaf Extract Mediated Synthesis of ZnO Nanoparticles: Characterization and Antimicrobial Activities. *Mater. Today: Proc.* **2020**, *23*, 73−80.
(65) Vijayakumar, S.; Vaseeharan, B.; Malaikozhundan, B.; Shobiya, M. Laurus Nobilis Leaf Extract Mediated Green Synthesis of ZnO Nanoparticles: Characterization and Biomedical Applications. *Biomed. Pharmacother.* **2016**, *84*, 1213−1222.
(66) Mohammadi Arvanag, F.; Bayrami, A.; Habibi-Yangjeh, A.; Rahim Pouran, S. A Comprehensive Study on Antidiabetic and Antibacterial Activities of ZnO Nanoparticles Biosynthesized Using Silybum Marianum L Seed Extract. *Mater. Sci. Eng. C* **2019**, *97*, 397−405.
(67) Salehi, B.; Martorell, M.; Arbiser, J. L.; Sureda, A.; Martins, N.; Maurya, P. K.; Sharifi-Rad, M.; Kumar, P.; Sharifi-Rad, J. Antioxidants : Positive or Negative Actors. *Biomolecules* **2018**, *8*, 124.
(68) Gulcin, I. Antioxidants and Antioxidant Methods : An Updated Overview. *Arch. Toxicol.* **2020**, *94*, 651−715.
(69) Das, D.; Nath, B.; Phukon, P.; Dolui, S. Synthesis and Evaluation of Antioxidant and Antibacterial Behavior of CuO Nanoparticles. *Colloids Surf., B* **2013**, *101*, 430−433.
(70) Lingaraju, K.; Raja Naika, H.; Manjunath, K.; Basavaraj, R. B.; Nagabhushana, H.; Nagaraju, G.; Suresh, D. Biogenic Synthesis of Zinc Oxide Nanoparticles Using Ruta Graveolens (L.) and Their Antibacterial and Antioxidant Activities. *Appl. Nanosci.* **2016**, *6*, 703−710.
(71) Nethravathi, P. C.; Shruthi, G. S.; Suresh, D.; Udayabhanu; Nagabhushana, H.; Sharma, S. C. Garcinia Xanthochymus Mediated Green Synthesis of ZnO Nanoparticles: Photoluminescence, Photocatalytic and Antioxidant Activity Studies. *Ceram. Int.* **2015**, *41*, 8680−8687.
(72) Sharmila, G.; Thirumarimurugan, M.; Muthukumaran, C. Green Synthesis of ZnO Nanoparticles Using Tecoma Castanifolia Leaf Extract: Characterization and Evaluation of Its Antioxidant, Bactericidal and Anticancer Activities. *Microchem. J.* **2019**, *145*, 578−587.
(73) Akhavan, O.; Ghaderi, E. Toxicity of Graphene and Graphene Oxide Nanowalls Against Bacteria. *ACS Nano* **2010**, *4*, 5731−5736.
(74) Dutta, T.; Sarkar, R.; Pakhira, B.; Ghosh, S.; Sarkar, R.; Barui, A.; Sarkar, S. ROS generation by Reduced Graphene Oxide (rGO) Induced by Visible Light Showing Antibacterial Activity : Comparison with Graphene Oxide (GO). *RSC Adv.* **2015**, *5*, 80192−80195.
(75) Prasanna, V. L.; Vijayaraghavan, R. Insight into the Mechanism of Antibacterial Activity of ZnO : Surface Defects Mediated Reactive Oxygen Species Even in the Dark. *Langmuir* **2015**, *31*, 9155−9162.
(76) Akhavan, O.; Ghaderi, E.; Esfandiar, A. Wrapping Bacteria by Graphene Nanosheets for Isolation from Environment , Reactivation by Sonication , and Inactivation by Near-Infrared Irradiation. *J. Phys. Chem. B* **2011**, *115*, 6279−6288.
(77) Hashemi, E.; Akhavan, O.; Shamsara, M.; Rahighi, R.; Esfandiar, A.; Tayefeh, A. R. Cyto and Genotoxicities of Graphene Oxide and Reduced Graphene Oxide Sheets on Spermatozoa. *RSC Adv.* **2014**, *4*, 27213−27223.
(78) Liu, S.; Zeng, T. H.; Hofmann, M.; Burcombe, E.; Wei, J.; Jiang, R.; Kong, J.; Chen, Y. Antibacterial Activity of Graphite , Graphite Oxide , Graphene Oxide , and Reduced Graphene Oxide : Membrane and Oxidative Stress. *ACS Nano* **2011**, *5*, 6971−6980.
(79) Akhavan, O.; Ghaderi, E.; Akhavan, A. Size-Dependent Genotoxicity of Graphene Nanoplatelets in Human Stem Cells. *Biomaterials* **2012**, *33*, 8017−8025.
(80) Song, W.; Zhang, J.; Guo, J.; Zhang, J.; Ding, F.; Li, L.; Sun, Z. Role of the Dissolved Zinc Ion and Reactive Oxygen Species in Cytotoxicity of ZnO Nanoparticles. *Toxicol. Lett.* **2010**, *199*, 389−397.
(81) Valdiglesias, V.; Costa, C.; Kiliç, G.; Costa, S.; Pásaro, E.; Laffon, B.; Teixeira, J. Neuronal Cytotoxicity and Genotoxicity Induced by Zinc Oxide Nanoparticles. *Environ. Int.* **2013**, *55*, 92−100.
(82) Akhavan, O.; Hashemi, E.; Zare, H.; Shamsara, M.; Taghavinia, N.; Heidari, F. Influence of Heavy Nanocrystals on Spermatozoa and Fertility of Mammals. *Mater. Sci. Eng. C* **2016**, *69*, 52−59.
(83) Jannesari, M.; Akhavan, O.; Madaah Hosseini, H. R. M.; Bakhshi, B. Graphene/CuO 2 Nanoshuttles with Controllable Release of Oxygen Nanobubbles Promoting Interruption of Bacterial Respiration. *ACS Appl. Mater. Interfaces* **2020**, *12*, 35813−35825.
(84) Sisubalan, N.; Ramkumar, V. S.; Pugazhendhi, A.; Karthikeyan, C.; Indira, K.; Gopinath, K.; Hameed, A. S. H.; Basha, M. H. G. ROS-Mediated Cytotoxic Activity of ZnO and CeO 2 Nanoparticles Synthesized Using the Rubia Cordifolia L. Leaf Extract on MG-63 Human Osteosarcoma Cell Lines. *Environ. Sci. Pollut. Res.* **2018**, *25*, 10482−10492.
(85) Nazar, N.; Bibi, I.; Kamal, S.; Iqbal, M.; Nouren, S.; Jilani, K.; Umair, M.; Ata, S. Cu Nanoparticles Synthesis Using Biological Molecule of P. Granatum Seeds Extract as Reducing and Capping

https://doi.org/10.1021/acsomega.2c07530
ACS Omega 2023, 8, 10954−10967

Agent: Growth Mechanism and Photo-Catalytic Activity. *Int. J. Biol. Macromol.* **2018**, *106*, 1203−1210.
(86) Abdullah, F. H.; Abu Bakar, N. H. H.; Abu Bakar, M. Low Temperature Biosynthesis of Crystalline Zinc Oxide Nanoparticles from Musa Acuminata Peel Extract for Visible-Light Degradation of Methylene Blue. *Optik* **2020**, *206*, 164279.
(87) Mirgane, N. A.; Shivankar, V. S.; Kotwal, S. B.; Wadhawa, G. C.; Sonawale, M. C. Degradation of Dyes Using Biologically Synthesized Zinc Oxide Nanoparticles. *Mater. Today: Proc.* **2021**, *37*, 849−853.
(88) Soto-Robles, C. A.; Nava, O.; Cornejo, L.; Lugo-Medina, E.; Vilchis-Nestor, A. R.; Castro-Beltrán, A.; Luque, P. A. Biosynthesis, Characterization and Photocatalytic Activity of ZnO Nanoparticles Using Extracts of Justicia Spicigera for the Degradation of Methylene Blue. *J. Mol. Struct.* **2021**, *1225*, 129101.

https://doi.org/10.1021/acsomega.2c07530
ACS Omega 2023, 8, 10954−10967